[NiFe] Hydrogenase

International Edition: DOI: 10.1002/anie.201508976
German Edition: DOI: 10.1002/ange.201508976

Krypton Derivatization of an O_2-Tolerant Membrane-Bound [NiFe] Hydrogenase Reveals a Hydrophobic Tunnel Network for Gas Transport

*Jacqueline Kalms, Andrea Schmidt, Stefan Frielingsdorf, Peter van der Linden, David von Stetten, Oliver Lenz, Philippe Carpentier, and Patrick Scheerer**

Abstract: *[NiFe] hydrogenases are metalloenzymes catalyzing the reversible heterolytic cleavage of hydrogen into protons and electrons. Gas tunnels make the deeply buried active site accessible to substrates and inhibitors. Understanding the architecture and function of the tunnels is pivotal to modulating the feature of O_2 tolerance in a subgroup of these [NiFe] hydrogenases, as they are interesting for developments in renewable energy technologies. Here we describe the crystal structure of the O_2-tolerant membrane-bound [NiFe] hydrogenase of Ralstonia eutropha (ReMBH), using krypton-pressurized crystals. The positions of the krypton atoms allow a comprehensive description of the tunnel network within the enzyme. A detailed overview of tunnel sizes, lengths, and routes is presented from tunnel calculations. A comparison of the ReMBH tunnel characteristics with crystal structures of other O_2-tolerant and O_2-sensitive [NiFe] hydrogenases revealed considerable differences in tunnel size and quantity between the two groups, which might be related to the striking feature of O_2 tolerance.*

The transport of reactants from the protein exterior to a buried active site or between multiple catalytic centers via protein tunnels is common to all six enzyme classes.[1,2] A particular remarkable example for the tunneling of intermediates is the class 6 enzyme carbamoyl phosphate synthetase. The three active sites are connected by two substrate tunnels spanning a total distance of almost 100 Å.[3] The access of the substrate to a buried active site has been studied in various enzymes, for example, bacteriorhodopsin, lipoxygenase, photosystem II, and hydrogenase.[4–9] Hydrogenases are metalloenzymes that catalyze the reaction $H_2 \rightleftharpoons H^- + H^+ \rightleftharpoons 2e^- + 2H^+$. They are widespread in all three domains of life and are classified according to the metal located at the active site. Members of the class of [Fe] hydrogenases catalyze a crucial step of methanogenesis in hydrogenotrophic archaea.[10] The [FeFe] hydrogenases are mostly involved in H_2 production under strictly anaerobic conditions, whereas [NiFe] hydrogenases are primarily H_2-oxidising enzymes.[11] [NiFe] hydrogenases can be further subdivided into O_2-sensitive and O_2-tolerant enzymes. O_2-sensitive hydrogenases are irreversibly inactivated in the presence of O_2, which is presumably caused by the reaction of reactive oxygen species with the metal cofactor(s).[12] In contrast, O_2-tolerant hydrogenases retain their enzymatic function in the presence of O_2,[13] which makes them attractive for biotechnological applications.[14] The feature of O_2 tolerance is related to the capability of the enzymes to use some of the electrons generated by H_2 oxidation for the complete reduction of O_2 to harmless water.[13,15] Prominent members of the O_2-tolerant enzymes belong to the group 1 membrane-bound [NiFe] hydrogenases (MBHs), which are made up of three subunits. The large subunit contains the [NiFe] active site where hydrogen splitting occurs and the small subunit harbors three [FeS] clusters that establish an electronic connection between the catalytic center and the third subunit, a membrane-integral cytochrome b_{562}. In this study we employed the catalytically active *Re*MBH heterodimer lacking cytochrome b_{562}.

According to the nature of the gas molecule approaching the [NiFe] active site via a hydrophobic tunnel, different enzymatic reactions take place. During the catalytic cycle H_2 is oxidized to protons and electrons. Protons are transported to the protein surface via protonatable amino acids and water molecules.[16] Electrons are guided through a relay composed of several iron–sulfur clusters to the primary electron acceptor.[17] In the event of O_2 approach, an additional reaction is proposed to occur at the [NiFe] active site. In this catalytic reactivation process, electrons are delivered from the electron relay to reduce O_2 with the aid of protons to H_2O, which then is released to the protein surface through a nearby water channel (Figure 1). Under aerobic conditions the [4Fe3S] cluster of the electron relay can undergo two redox transitions at physiological potential and transfers a second electron to the active site. In this two-electron mode structural changes occur at this cluster and one iron ion (Fe4) changes its binding partners (iron shift).[18] The crystal structures available so far for *Re*MBH[17,18] revealed plausible pathways for electron transport and water release, while both the proton pathways and gas transport routes remained largely unde-

[*] J. Kalms, A. Schmidt, Dr. P. Scheerer
Institut für Medizinische Physik und Biophysik (CC2)
Group Protein X-ray Crystallography and Signal Transduction
Charité – Universitätsmedizin Berlin
Charitéplatz 1, 10117 Berlin (Germany)
E-mail: patrick.scheerer@charite.de
Dr. S. Frielingsdorf, Dr. O. Lenz
Institut für Chemie, Sekr. PC14
Technische Universität Berlin
Strasse des 17. Juni 135, 10623 Berlin (Germany)
P. van der Linden, Dr. D. von Stetten, Dr. P. Carpentier
ESRF—European Synchrotron Radiation Facility
71 Avenue des Martyrs, Grenoble Cedex 9, 38043 (France)

Supporting information for this article can be found under http://dx.doi.org/10.1002/anie.201508976.

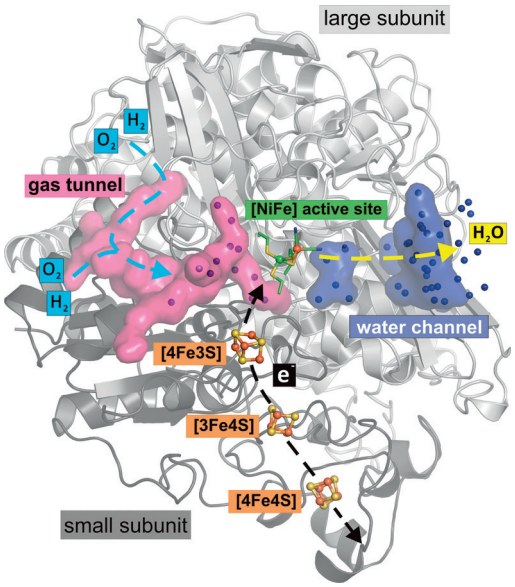

Figure 1. Ribbon representation of the large and small subunit of *Re*MBH (PDB entry: 3RGW) with the [NiFe] active site and its [FeS] clusters (proximal: [4Fe3S], medial: [3Fe4S], distal: [4Fe4S]) shown as balls and sticks. The gas tunnel (magenta) and the water channel (blue) are depicted as surfaces (calculated for all figures with PyMOL).[20] Water molecules (spheres) of the tunnel and channel are shown in the corresponding color (magenta/blue). The routes for H_2/O_2 and H_2O through the tunnels/channels are indicated by the light-blue and yellow arrows, respectively. The electron flow is represented by black arrows.

fined. Efficient gas transport to the deeply buried active site requires a tunnel that connects the protein exterior with the catalytic center.[19]

In 1997, a gas tunnel was proposed based on the derivatization with xenon (Xe) gas in crystals of O_2-sensitive [NiFe] hydrogenase from *Desulfovibrio fructosovorans* (*Df*).[9] Here we present high-resolution X-ray data of the O_2-tolerant *Re*MBH with multiple krypton (Kr) binding sites according to which a hydrophobic gas tunnel was defined. The hydrophobicity and high atomic number of noble gases like Kr and Xe make them favorable for the investigation of hydrophobic gas tunnels in pressurization experiments and X-ray studies.[4,6–9] A comparison of the gas tunnel architectures derived from crystal structures of O_2-sensitive and O_2-tolerant [NiFe] hydrogenases of various organisms uncovered significant differences, which are discussed in light of the O_2 tolerance of some [NiFe] hydrogenases.

In order to track the location of the hydrophobic gas tunnel we used the efficient method of noble gas derivatization of *Re*MBH crystals. Several native and anomalous data sets were collected (high-resolution and anomalous datasets at 1.47 Å and 2.52 Å resolution, respectively; see Table S1 in the Supporting Information). The overall protein structure of the krypton-derivatized *Re*MBH, including the four metal cofactors, is structurally identical to that of the as-isolated ("oxidized state 2") wildtype enzyme.[18] The [NiFe] active site resides in the so-called Ni_r-B state, characterized by an OH^- ligand bridging the two metals. The corresponding Ni–Fe distance is 2.85 Å. The structure of the [4Fe3S] cluster, however, shows some heterogeneity as the iron ion (Fe_4) involved in the iron-shift was found in a double conformation, which is reflected by an extended electron density (Figure S1). The increased flexibility might be caused by the noble gas derivatization method. However, the cluster structure is certainly no mixture of the previously reported H_2-reduced and "oxidized state 2", because both Fe_4 positions in the current structure are close to the position found in the "oxidized state 2".[18] The *Re*MBH structure contains 19 Kr sites with different occupancies located in tunnels and cavities (Table S2 and Figure S2). 15 out of 19 krypton atoms form an apparent hydrophobic gas tunnel network that connects the protein surface with the [NiFe] active site (Figure 2). Water

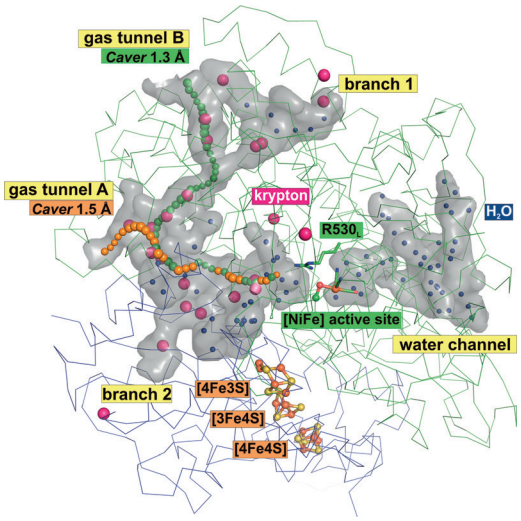

Figure 2. Stick representation of the large and small subunit of krypton-derivatized *Re*MBH (PDB entry: 5D51). The [NiFe] active site and the [FeS] clusters are shown as balls and sticks. The hydrophobic gas tunnel and the water channel are depicted as gray surfaces. Krypton atoms (magenta) and water molecules (blue) are shown as single spheres. $R530_L$ served as the initial starting point for *Caver* calculations. The results are represented by green and orange chains with a bottleneck radius of 1.3 Å and 1.5 Å, respectively.

molecules are located in hydrophilic cavities that form a water channel, which links the catalytic center with the protein exterior (Figure 2). The gas can enter the hydrophobic tunnel network through two openings, gas tunnels A and B, at the enzyme surface (Figure 2). Montet et al.[9] showed previously two main inlets for Xe and H_2 in the *Df*-[NiFe] hydrogenase, which are partially in agreement with the tunnel entrances of *Re*MBH. The proposed main inlet in channel b-a of *Df*-hydrogenase was found blocked in *Re*MBH (branch 2), whereas the second entrance located in channel c corresponds to the gas tunnel A entrance in our structure (Figure 2). The second gas tunnel opening in *Re*MBH (gas tunnel B) refers to channel f-d in the *Df* enzyme, which was reported as a functionally unimportant path for gas diffusion.[9] The 10 Xe sites identified by Montet et al. appear to occupy the same hydrophobic pathways that were revealed by krypton derivatization in our study.

To further support our experimental results, tunnel calculations were conducted with the program *Caver*.[20] We

performed the analysis with a minimal probe radius of 1.2 Å, which corresponds to the van der Waals radius of hydrogen (Table S3). The tunnel prediction with *Caver* was carried out in 0.1 Å steps up to 1.6 Å, which was the largest value showing tunnels. The invariant amino acid residue $R530_L$ (*Re*MBH nomenclature: L = large and S = small subunit), which is located in close proximity to the [NiFe] active site, served as the initial starting point for the tunnel calculations (Figure 2). This particular arginine is conserved among the [NiFe] hydrogenases known so far.[17,21]

The calculations revealed two plausible tunnel pathways in *Re*MBH, which are in agreement with the position of the krypton atoms (Figure 2). Gas tunnel A is 30 Å in length with a maximum bottleneck radius (narrowest part of a given tunnel)[20] of 1.5 Å. The gas tunnel B is 50 Å long with a bottleneck radius of 1.3 Å (Figure 2 and Table S4). The calculated routes are in full agreement with the chain of krypton atoms in the *Re*MBH structure. Subsequently, we examined the crystal structures of various group 1 hydrogenases for the presence of possible gas tunnels calculated with *Caver*. For that purpose the O_2-tolerant enzymes from *Ralstonia eutropha* (*Re*), *Escherichia coli* (*EcHyd-1*), *Hydrogenovibrio marinus* (*Hm*), and *Salmonella enterica* (*Se*) were compared to the O_2-sensitive hydrogenases from *Desulfovibrio gigas* (*Dg*), *Desulfovibrio desulfuricans* (*Dd*), *Desulfovibrio vulgaris* (*Dv*), *Desulfovibrio fructosovorans* (*Df*), and *Allochromatium vinosum* (*Av*) (Tables S4 and S5). A comparison of gas tunnel networks of O_2-tolerant and O_2-sensitive hydrogenases is exemplified by *Re*MBH and *Dv* hydrogenase (Figure 3). Although substantial sections of the gas tunnel network seem to be conserved (Figure 3), there are significant differences between the hydrogenases regarding the number of tunnels leading to the protein surface (see Tables S4 and S5). O_2-tolerant hydrogenases contain on average only two tunnels; the only exception is *Hm*MBH,[22] which harbors three and four tunnel openings for the H_2-reduced and air-oxidized states, respectively. The tunnel bottleneck radii range between 1.2 Å and 1.5 Å. Thus, there is a remarkable congruence concerning the number of gas tunnels (ca. two) in O_2-tolerant [NiFe] hydrogenases. A similar consistency holds true for O_2-sensitive enzymes. Except for *Dd* hydrogenase[23] with only two tunnels, the other four analyzed enzymes contain at least five tunnel openings. The corresponding bottleneck radii range between 1.2 Å and 1.6 Å.

In conclusion, the occurrence of hydrophobic tunnels and openings in O_2-sensitive hydrogenases is on average two times higher than in their O_2-tolerant counterparts (Tables S4 and S5). Although *Hm*MBH, *Ec*Hyd-1,[24] and *Dd* hydrogenase show a tunnel network similar to that of their consensus counterparts, there is a considerable difference in the number of tunnel openings. Branches 1 and 2 (Figure 2), which are open for gas access in all studied O_2-sensitive enzymes (Figure 3), are blocked in *Dd* hydrogenase. O_2-tolerant *Hm*MBH contains openings for the two gas tunnels at the end of branches 1 and 2. According to the calculations, *Ec*Hyd-1 has only one opening located at gas tunnel A (Figure 4). The fact that gas tunnel A seems to be present in all O_2-tolerant and O_2-sensitive [NiFe] hydrogenases leads to the conclusion that this tunnel is mainly used for gas transport

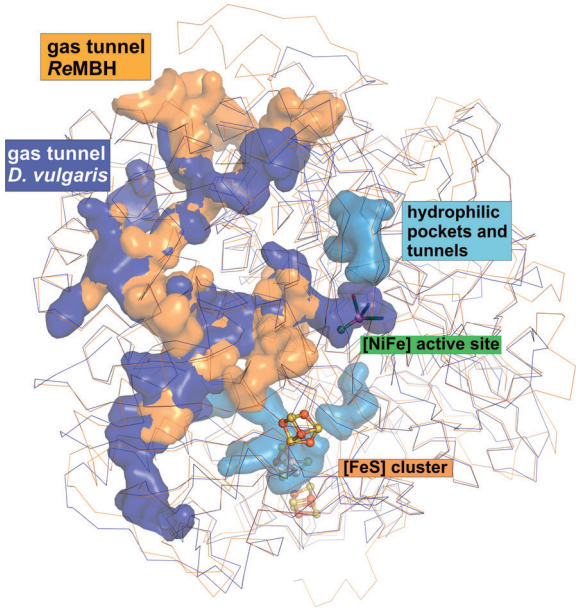

Figure 3. Stick representation of the O_2-tolerant *Re*MBH (PDB entry: 3RGW, orange) and O_2-sensitive *Dv* hydrogenase[27] (PDB entry: 1WUL, dark blue). The [FeS] clusters and the [NiFe] active site are illustrated as balls and sticks. The hydrophobic gas tunnels in *Re*MBH (in orange) and *Dv* (in dark blue) are also shown. Hydrophilic pockets and tunnels of *Dv* hydrogenase are depicted in light blue.

(Figure 2). Differences between the hydrogenases are also manifested in the gas tunnel dimensions. The majority of the tunnels present in O_2-tolerant and O_2-sensitive enzymes feature a bottleneck radius of 1.2 Å (37.5%) and 1.3 Å

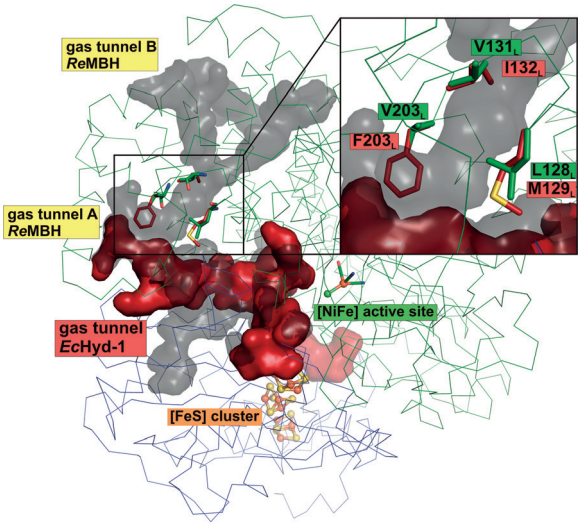

Figure 4. Superposition of the hydrophobic tunnels from *Re*MBH (PDB entry: 3RGW, gray) and *Ec*Hyd-1 (PDB entry: 3UQY, dark red). The protein backbone of *Re*MBH and the four metal cofactors shown as balls and sticks. The superposed gas tunnels are depicted as surfaces. Close-up view: The three *Ec*Hyd-1 amino acids ($M129_L$, $I132_L$, $F203_L$) blocking gas tunnel B are shown as dark-red sticks. They are superposed with the *Re*MBH amino acids $L128_L$, $V131_L$, $V203_L$ (green sticks).

(43.5%), respectively, and they span distances of 28–76 Å between the protein surface and the reactive center. However, on average the tunnels with the largest bottleneck have the shortest length. As evident in Figure 2, the *Re*MBH gas tunnel A has the largest bottleneck radius of 1.5 Å and a short length of 30 Å; in contrast, gas tunnel B is 50 Å in length and has a bottleneck radius of just 1.3 Å. The gas tunnel dimensions in all other studied structures (except *Dv* hydrogenase[25]) show a similar relation. As mentioned above, there is a considerable conformity of the gas tunnel architecture in O_2-tolerant and O_2-sensitive [NiFe] hydrogenases, particularly in close proximity to the active site. According to our calculations, the calculated starting point of the tunnel is situated 3–4 Å away from the conserved arginine residue ($R530_L$ in the case of *Re*MBH; Figure 2). An increase in the bottleneck radius would lead to a greater maximum distance between initial and calculated starting point. This implies that the end of the gas tunnel close to the active site is getting narrower. Such an effect has already been observed for *Df* hydrogenase carrying amino acid substitutions at the proposed active site gate (Table S6).[26] Moreover, a previous study demonstrated that an expansion by site-directed amino acid replacements of the potential gas tunnel of the H_2-sensing regulatory hydrogenase of *Re* yielded variants that are sensitive to inhibition by O_2.[27] In *Df* hydrogenase, replacement of the highly conserved residues, $V74_L$ and $L122_L$, by $M74_L/M122_L$ (PDB entry: 3CUR) and $I74_L/F122_L$ (PDB entry: 3CUS) led to a shift of the calculated starting point of the tunnel of 9 Å away from $R530_L$, due to the steric bulk of the amino acid side groups (Figure S3).[26] We used the corresponding crystal structures to calculate a virtual gas tunnel at 3 Å maximum distance to the conserved arginine. This calculation revealed a tunnel bottleneck radius of only 1 Å, which makes it rather difficult for O_2 and even H_2 to reach the active site.

This assumption is indeed reflected by a substantial increase in the Michaelis constant for H_2 in the case of the $V74_LI/L122_LF$ ($K_mH_2 = 50$ μM) and $V74_LM/L122_LM$ ($K_mH_2 = 200$ μM) variants compared to the native *Df* hydrogenase ($K_mH_2 = 10$ μM).[26] The single amino acid substitutions led to a maximum distance similar to that of the native structure (Table S6). The crystal structures indicate a slightly larger distance between the conserved gate residues, valine and leucine, in O_2-tolerant hydrogenases than in O_2-sensitive enzymes. This is mainly due to conformational differences of residue $L125_L$ (*Re*MBH nomenclature) (Figure S4). The experimental data of double-exchange variants of *Df* hydrogenase and the *Caver* calculations demonstrate that an exchange of the active-site gate amino acids to bulkier residues and the diameter of the gas tunnel ending have a major impact on the gas flow to the active site. Intriguingly, there is more variability in amino acids involved in tunnel formation within the group of O_2-sensitive hydrogenases than we observe in O_2-tolerant hydrogenases. Both groups show an amino acid invariance of 37.4% within conserved tunnel structures (Figures S7 and S8).

Additionally, we identified a hydrophilic tunnel directly at the medial [3Fe4S] cluster exclusively in the O_2-sensitive hydrogenases. This tunnel is blocked by a tryptophan in O_2-tolerant hydrogenases, which replaces a phenylalanine present in O_2-sensitive enzymes (except for the *Av* hydrogenase[28]) (Figures S5 and S6). Blocking the [3Fe4S] cluster to solvent accessibility might influence the electrochemical potential of the cluster.[29] In the case of O_2-tolerant enzymes only *Ec*Hyd-1 shows major differences in amino acid composition of the gas tunnel network. The bulkier amino acids $F203_L$, $M129_L$, and $I132_L$ block the gas tunnel B (Figure 4, Table S7).[24] The main gas tunnel A has a bottleneck radius of 1.2 Å and is 32 Å in length.

Based on the positioning of the krypton atoms in the hydrophobic tunnels of *Re*MBH and the corresponding theoretical prediction of gas tunnel routes in both O_2-sensitive and O_2-tolerant [NiFe] hydrogenases, we hypothesize that the O_2-sensitive enzymes have a more complex tunnel network and more openings than their O_2-tolerant counterparts. This may lead to increased gas diffusion rates for both H_2 and inhibitory gases such as O_2 and CO. In comparison, the gas tunnels of O_2-tolerant hydrogenases seem narrow and have fewer openings. This property presumably limits the gas flow rate to the catalytic center, which in turn may contribute to the remarkable O_2 tolerance of these enzymes. We would like to emphasize that the results of this study are based on the analyses of static crystal structures. However, dynamic changes of the gas tunnel networks are likely affecting gas access to the active site, and molecular dynamics (MD) simulations represent an invaluable tool to investigate such effects in future studies. Our krypton-pressurized *Re*MBH crystal structure therefore represents an excellent starting point for comprehensive MD simulations in order to investigate gas diffusion processes in relation to continuous changes in the gas tunnel diameters. In addition, investigating *Re*MBH variants providing gas tunnel modifications could be helpful to further prove our hypothesis.

Experimental Section

*Re*MBH was produced and purified as described previously.[17] Optimized *Re*MBH crystals were obtained using sitting-drop vapor diffusion[17,18] and were krypton-pressurized with a high-pressure cooling system.[30] A detailed description of all experiments can be found in the Supporting Information.

Acknowledgements

We are grateful to the scientific staff of the European Synchrotron Radiation Facility (ESRF, Grenoble, France) at beamlines ID14-1, ID23-1, ID23-2, ID14-4, and ID29, where the data were collected, for continuous support. We like to thank Ciara Lally for critically reading the manuscript. This work was supported by grants from the Deutsche Forschungsgemeinschaft (SFB740-B6 to P.S.; SFB1078-B6 to P.S.), ESRF (to P.v.d.L., D.v.S., and P.C., and P.S.), DFG Cluster of Excellence "Unifying Concepts in Catalysis" (Research Field E3-1 to J.K., A.S., S.F., O.L., and P.S.).

Keywords: hydrogenases · krypton · metalloenzymes · oxygen · structural biology

How to cite: *Angew. Chem. Int. Ed.* **2016**, *55*, 5586–5590
Angew. Chem. **2016**, *128*, 5676–5680

[1] L. J. Kingsley, M. A. Lill, *Proteins Struct. Funct. Bioinf.* **2015**, *83*, 599–611.
[2] F. M. Raushel, J. B. Thoden, H. M. Holden, *Acc. Chem. Res.* **2003**, *36*, 539–548.
[3] A. Weeks, L. Lund, F. M. Raushel, *Curr. Opin. Chem. Biol.* **2006**, *10*, 465–472.
[4] N. Hayakawa, T. Kasahara, D. Hasegawa, K. Yoshimura, M. Murakami, T. Kouyama, *J. Mol. Biol.* **2008**, *384*, 812–823.
[5] J. Saam, I. Ivanov, M. Walther, H. G. Holzhütter, H. Kuhn, *Proc. Natl. Acad. Sci. USA* **2007**, *104*, 13319–13324.
[6] J. W. Murray, J. Barber, *J. Struct. Biol.* **2007**, *159*, 228–237.
[7] A. Guskov, J. Kern, A. Gabdulkhakov, M. Broser, A. Zouni, W. Saenger, *Nat. Struct. Mol. Biol.* **2009**, *16*, 334–342.
[8] A. Gabdulkhakov, A. Guskov, M. Broser, J. Kern, F. Müh, W. Saenger, A. Zouni, *Structure* **2009**, *17*, 1223–1234.
[9] Y. Montet, P. Amara, A. Volbeda, X. Vernede, E. C. Hatchikian, M. J. Field, M. Frey, J. C. Fontecilla-Camps, *Nat. Struct. Biol.* **1997**, *4*, 523–526.
[10] C. Zirngibl, W. van Dongen, B. Schwörer, R. von Bünau, M. Richter, A. Klein, R. K. Thauer, *Eur. J. Biochem.* **1992**, *208*, 511–520.
[11] W. Lubitz, H. Ogata, O. Rüdiger, E. Reijerse, *Chem. Rev.* **2014**, *114*, 4081–4148.
[12] J. C. Fontecilla-Camps, A. Volbeda, C. Cavazza, Y. Nicolet, *Chem. Rev.* **2007**, *107*, 4273–4303.
[13] P. Wulff, C. C. Day, F. Sargent, F. A. Armstrong, *Proc. Natl. Acad. Sci. USA* **2014**, *111*, 6606–6611.
[14] B. Friedrich, J. Fritsch, O. Lenz, *Curr. Opin. Biotechnol.* **2011**, *22*, 358–364.
[15] L. Lauterbach, O. Lenz, *J. Am. Chem. Soc.* **2013**, *135*, 17897–17905.
[16] V. H. Teixeira, C. M. Soares, A. M. Baptista, *Proteins Struct. Funct. Bioinf.* **2008**, *70*, 1010–1022.
[17] J. Fritsch, P. Scheerer, S. Frielingsdorf, S. Kroschinsky, B. Friedrich, O. Lenz, C. M. Spahn, *Nature* **2011**, *479*, 249–252.
[18] S. Frielingsdorf, J. Fritsch, A. Schmidt, M. Hammer, J. Löwenstein, E. Siebert, V. Pelmenschikov, T. Jaenicke, J. Kalms, Y. Rippers, F. Lendzian, I. Zebger, C. Teutloff, M. Kaupp, R. Bittl, P. Hildebrandt, B. Friedrich, O. Lenz, P. Scheerer, *Nat. Chem. Biol.* **2014**, *10*, 378–385.
[19] J. C. Fontecilla-Camps, P. Amara, C. Cavazza, Y. Nicolet, A. Volbeda, *Nature* **2009**, *460*, 814–822.
[20] B. Kozlíková, E. Šebestová, V. Šustr, J. Brezovský, O. Strnad, L. Daniel, D. Bednář, A. Pavelka, M. Maňák, M. Bezděka, P. BeneŠ, M. Kotry, A. W. Gora, J. Damborský, J. Sochor, *Bioinformatics* **2014**, *30*, 2684–2685.
[21] C. Greening, A. Biswas, C. R. Carere, C. J. Jackson, M. C. Taylor, M. B. Stott, G. M. Cook, S. E. Morales, *ISME J.* **2016**, *10*, 761–777.
[22] Y. Shomura, K. S. Yoon, H. Nishihara, Y. Higuchi, *Nature* **2011**, *479*, 253–256.
[23] P. M. Matias, C. M. Soares, L. M. Saraiva, R. Coelho, J. Morais, J. Le Gall, M. A. Carrondo, *J. Biol. Inorg. Chem.* **2001**, *6*, 63–81.
[24] A. Volbeda, P. Amara, C. Darnault, J. M. Mouesca, A. Parkin, M. M. Roessler, F. A. Armstrong, J. C. Fontecilla-Camps, *Proc. Natl. Acad. Sci. USA* **2012**, *109*, 5305–5310.
[25] H. Ogata, S. Hirota, A. Nakahara, H. Komori, N. Shibata, T. Kato, K. Kano, Y. Higuchi, *Structure* **2005**, *13*, 1635–1642.
[26] F. Leroux, S. Dementin, B. Burlat, L. Cournac, A. Volbeda, S. Champ, L. Martin, B. Guigliarelli, P. Bertrand, J. C. Fontecilla-Camps, M. Rousset, C. Léger, *Proc. Natl. Acad. Sci. USA* **2008**, *105*, 11188–11193.
[27] T. Buhrke, O. Lenz, N. Krauss, B. Friedrich, *J. Biol. Chem.* **2005**, *280*, 23791–23796.
[28] H. Ogata, P. Kellers, W. Lubitz, *J. Mol. Biol.* **2010**, *402*, 428–444.
[29] A. Dey, F. E., Jr. Jenney, M. W. Adams, E. Babini, Y. Takahashi, K. Fukuyama, K. O. Hodgson, B. Hedman, E. I. Solomon, *Science* **2007**, *318*, 1464–1468.
[30] P. van der Linden, F. Dobias, H. Vitoux, U. Kapp, J. Jacobs, S. Mc Sweeney, C. Mueller-Dieckmann, P. Carpentier, *J. Appl. Crystallogr.* **2014**, *47*, 584–592.

Received: September 24, 2015
Revised: December 17, 2015
Published online: February 23, 2016

